

RSC Advances



This is an *Accepted Manuscript*, which has been through the Royal Society of Chemistry peer review process and has been accepted for publication.

Accepted Manuscripts are published online shortly after acceptance, before technical editing, formatting and proof reading. Using this free service, authors can make their results available to the community, in citable form, before we publish the edited article. This *Accepted Manuscript* will be replaced by the edited, formatted and paginated article as soon as this is available.

You can find more information about *Accepted Manuscripts* in the [Information for Authors](#).

Please note that technical editing may introduce minor changes to the text and/or graphics, which may alter content. The journal's standard [Terms & Conditions](#) and the [Ethical guidelines](#) still apply. In no event shall the Royal Society of Chemistry be held responsible for any errors or omissions in this *Accepted Manuscript* or any consequences arising from the use of any information it contains.

A simple hydrothermal route for the preparation of HgS nanoparticles and their photocatalytic activities

Rengaraj Selvaraj^{a*}, Kezhen Qi^b, Salma M. Z. Al-Kindy^a, Mika Sillanpää^c, Younghun Kim^d, Cheuk-wai Tai^e

5

Received (in XXX, XXX) Xth XXXXXXXXX 200X, Accepted Xth XXXXXXXXX 200X

First published on the web Xth XXXXXXXXX 200X

DOI: 10.1039/b000000x

HgS nanoparticles have been successfully prepared by a hydrothermal method using polyethylene glycol (PEG) as stabilizing agent and characterized by a variety of methods. Our experiments confirmed that the size of the HgS nanocrystal could be easily modified by turning the chain length of PEG. X-ray powder diffraction (XRD) results of the nanoparticles revealed that the hexagonal structure of the HgS, i.e. α -phase known as cinnabar. Morphological studies performed by scanning electron microscopy (SEM) and transmission electron microscopy (TEM) showed the synthesized nanocrystals were nanoparticles. Furthermore, a rational mechanism to the formation and evolution of the products is proposed. The optical properties of HgS were investigated by diffuse reflectance spectrum (DRS), which indicated that the band gap of the nanoparticles is slightly decreased from 2.05 to 2.00 eV as the average particle size decreasing from 55 to 35 nm. Furthermore, the photocatalytic activity studies of the particles demonstrated their excellent photocatalytic performance in rapidly degrading aqueous methylene blue dye solution under visible light irradiation. These results suggest that HgS nanoparticles will be an interesting candidate of photocatalyst working in visible light range.

20

1. Introduction

The rational design and fabrication of nanomaterials with special morphology have attracted a great deal of attention because the properties of material depend not only on its chemical composition and phase, but also depend on its shape and size.¹ Particularly, the synthesis of semiconductor nanomaterial with different sizes has motivated much attention due to its size-dependent properties, and potential applications in the fields of optics, catalysts, electronics, and so on.² Therefore, various approaches have been developed to synthesize nanocrystals with controlled morphology,³ among which the hydrothermal method is considered to be efficient,⁴ because it is demonstrated to be effective for controlling the shape and size of nanomaterials.

Sulfides of metal have been extensively investigated due to their promising properties and potential use in many devices.⁵ Among the metal sulfides, mercury (II) sulfide (HgS) is widely used in many fields such as infrared sense and emitter,⁶ electrostatic image materials,⁷ semiconductor,⁸ optical applications,⁹ and photoelectric conversion devices.¹⁰ These applications are resulted from its unique physicochemical properties, which depend not only on the phase but also on the shape and size. For instance, Higginson *et al.*, demonstrated that the HgS crystals exhibit different optical properties corresponding to their different shape and size changes.¹¹ Over the past few years, great effort has been made to control the synthesis of HgS nanomaterial, many different HgS morphologies have been

reported, such as nanoparticle,¹² nanorod,¹³ nanowire,¹⁴ nanodendrite,¹⁵ and nanotubule.¹⁶ However, the development of facile, mild and effective methods for synthesis of HgS nanocrystals with a controllable size and morphology is still a great challenge.

In this work, we present a simple hydrothermal synthesis of HgS nanocrystals using PEG as stabilizing agent. It is found that the morphology variations of the HgS nanoparticles were achieved by simply varying the PEG length. Namely, the size of HgS particles is decreased by increasing the PEG length. Furthermore, a rational mechanism to the formation and evolution of the products is proposed. The diffuse reflectance spectrum (DRS) measurements showed that these HgS samples have the band gap from 2.05 to 2.00 eV. These HgS nanoparticles could be potentially applied to photocatalytic degradation studies. The photocatalytic activity of as-prepared HgS nanoparticles was also evaluated by using methylene blue dye solution as a model organic compound and the result revealed that the product as-obtained had good photocatalytic activity.

2. Experimental Section

2.1 Synthesis of HgS nanocrystal.

The HgS nanocrystals were prepared using analytical grade, mercury (II) nitrate ($\text{Hg}(\text{NO}_3)_2 \cdot 4\text{H}_2\text{O}$ (Sigma-Aldrich 99%), thioacetamide ($\text{C}_2\text{H}_5\text{NS}$) (Sigma-Aldrich 99%) and poly(ethylene glycol) (PEG) (Merck, Germany). In a typical synthesis, 3.24 mmol of $\text{Hg}(\text{NO}_3)_2 \cdot 4\text{H}_2\text{O}$, 5.32 mmol of Thioacetamide (TAA) and 0.6 g of PEG (PEG-0, 2000, 4000, and 6000) were dissolved

in 50 mL of deionized water to form the reaction solution. The mixture was continuously stirred for 30 min at room temperature, and then was transferred into an autoclave with a Teflon lining and heated at 180°C for 10 h, and then allowed to cool to room temperature. The as-prepared product was separated by centrifugation, washed several times with deionized water and ethanol respectively, and dried at 60°C for 24 h. Finally, the products were calcined at 350°C for 2 h for further characterization.

2.2 Characterization of HgS nanoparticles.

The products were characterized by X-ray diffraction (XRD) using a Bruker (D5005) X-ray diffractometer equipped with graphite monochromatized CuK α radiation ($\lambda = 1.54056 \text{ \AA}$). The morphology of the as-synthesized products was examined by scanning electron microscopy (SEM). The SEM measurements were performed with a Hitachi S-4800 high-resolution field-emission scanning electron microscope (HR-SEM), which is equipped with an energy dispersive X-ray spectrometer (EDX). The morphology of the products was also carried out in transmission electron microscope (JEOL JEM-3010). The chemical states and the relative composition of the samples were studied by X-ray photoelectron spectroscopy (XPS), which is a highly surface sensitive technique with information depth in a few nanometers. The X-ray source is Al K α radiation (1.486.7 eV). The photo-emitted electrons escaped from the sample were analyzed in a hemispherical energy analyzer at a pass energy of $E_p = 20 \text{ eV}$. All spectra were obtained with an energy step of 0.1 eV and a dwell time of 50 ms. A software package (Avantage Thermo VG) was used to analyze the XPS data and fit the curves. The absorption spectrum of the samples in the diffused reflectance spectrum (DRS) mode was recorded in the wavelength range between 200 and 1000 nm using a spectrophotometer (Jasco-V670), with BaSO $_4$ as a reference. From the absorption edge, the band gap values were calculated by extrapolation.

All photoreaction experiments were carried out in a photocatalytic reactor system, which consists of a cylindrical borosilicate glass reactor vessels with an effective volume of 500 mL, a cooling water jacket, and a 150 W sodium vapour lamp (OSRAM Vialox NAV-TS Super 150 W) positioned axially at the center as a visible light source. The reaction temperature was kept at 20°C by cooling water. A special glass frit as an air diffuser was fixed at the reactor to uniformly disperse air into the solution.

Visible light photocatalytic activity studies were performed to examine the methylene blue (MB) degradation in an aqueous solution. For each run the reaction suspensions were freshly prepared by adding 0.10 g of catalyst into 250 mL of aqueous methylene blue solution, with an initial concentration of 5 mg L $^{-1}$. Prior to the photoreaction, the suspension was magnetically stirred in a dark condition for 30 min to attain the adsorption/desorption equilibrium condition. The aqueous suspension containing methylene blue and photocatalyst was then irradiated with visible light with constant aeration. At the given time intervals, the analytical samples were taken from the suspension, immediately centrifuged at 4000 revolutions per minute (rpm) for 15 min, and then filtered to remove the catalyst. The filtrate was analysed by an ultraviolet-visible (UV-vis)

absorption spectra instrument (Perkin-Elmer Lambda 45 UV-vis spectrometer) to understand the methylene blue degradation. The degree of degradation has been derived from the UV-vis absorption intensity, which has been integrated at the wavelength of 664 nm.

3. Results and Discussion

3.1 Structure and composition determination

The XRD patterns of the samples prepared in different length of PEG are shown in Fig. 1. All diffraction peaks in the patterns can be indexed to be a pure hexagonal phase (α -phase) HgS (JCPDS card no. 6-0256). It is worth to note that similar XRD patterns were observed for all samples prepared with different PEG lengths, indicating that changing PEG length does not change the phase and crystallinity of HgS.

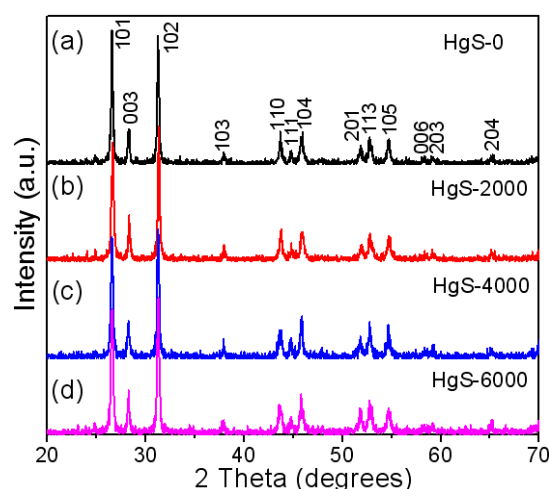


Fig. 1. XRD patterns of the as-prepared HgS products with different PEG lengths (a) PEG-0, (b) PEG-2000, (c) PEG-4000, and (d) PEG-6000.

To confirm the composition of the samples (HgS-PEG-2000 sample, for example), XPS analysis was carried out, as shown in Fig. 2. The binding energies obtained in the XPS analysis are corrected for specimen charging by referencing the C1s to 285.2 eV. The wide XPS spectrum was shown in Fig. 2a. No peaks of other elements except C, O, Hg, and S were observed. The observed C peak is due to the carbon supporting film on the copper TEM grid, and the O peaks can be attributed to the absorption of oxygen on the sample surface. The XPS spectra of HgS sample was consistent with the typical HgS spectrum reported in the literature.¹⁷ Figures 2b and 2c showed the high-resolution XPS spectra of Hg 4f and S 2p, respectively. The two strong peaks taken for the Hg region at 99.4 and 103.3 eV were assigned to the Hg 4f binding energy. The peaks measured in the S energy region detected at 160.7 and 161.5 eV were attributed to the S 2p transitions. These values are in good agreement with the reported data.¹⁸ According to the measurements of the Hg 4f and S 2p peak areas, the atomic ratio of Hg : S is 1.07:1, very close to the composition of HgS.

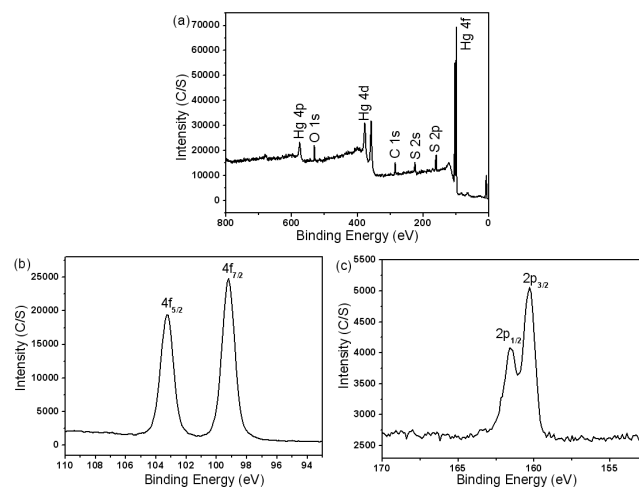


Fig. 2. XPS analysis of the sample HgS-PEG-2000: (a) survey spectrum, (b) Hg 4f bonding-energy spectrum, and (c) S 2p bonding-energy spectrum.

3.2 Morphology of samples

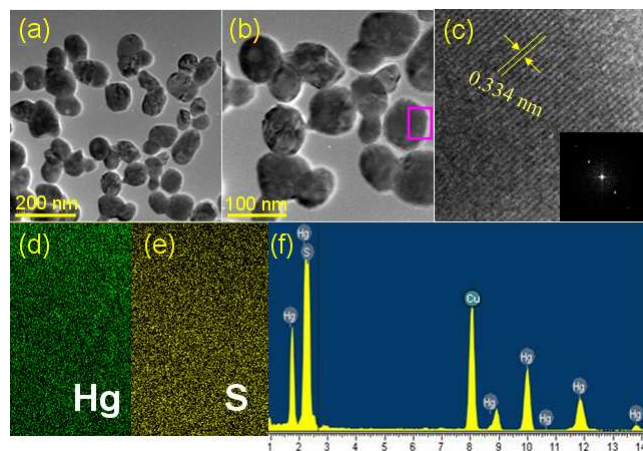


Fig. 3. The morphology and structure of as-prepared HgS nanoparticles by PEG-2000 assistance. (a) low-, and (b) high-magnification TEM images; (c) HRTEM image of the selected area marked with a pink square in (b); the inset is the corresponding fast Fourier transformation (FFT) pattern; (d, e) the corresponding EDS elemental mapping images of Hg and S. (f) EDX spectrum of the HgS nanoparticles.

Morphologies of the HgS nanocrystals prepared in different PEG lengths under the same reaction condition that is the reaction temperature kept at 180°C for 10 hours and the molar ratio of $\text{Hg}^{2+}/\text{S}^{2-}$ at 1:1. As an example, when PEG-2000 is employed, the product is comprised of nanoparticles with a diameter of 30-50 nm (Fig. 3a), which agrees well the value of crystalline size based on the Scherrer Formula, from the XRD data. The HRTEM image of the edge of the single nanoparticle (Fig. 3b) marked by a square in Fig. 3c shows that the distance between adjacent lattice planes is about 0.33 nm, corresponding to the (101) plane, indicating that the final HgS nanoparticle exhibits a preferred growth along the [101] direction. The EDX image recorded from the same region also confirms that the components of the products are only Hg and S with a ratio of 1.03 : 1 (Fig. 3f), which is supported by the element map (Figures 3d and 3e). The Cu signal is attributed to the copper supporting grid.

The morphology of the samples with different PEG lengths is

further examined by SEM (Fig. 4). When PEG-2000 was used, the diameters of the as-obtained HgS nanoparticles are 40-60 nm (Fig. 4b). When the PEG length is decreased to PEG-0, the diameters are dispersed more from 40 to 70 nm (Fig. 4a). When the PEG-2000 further increase to PEG-4000, the diameter disperse rang is back to 30-50 nm (Fig. 4c). When PEG-6000 is employed, the product is comprised of the smallest nanoparticles illustrated in Fig. 4, about 25-45 nm. The results indicate that the size of HgS nanoparticles can be easily controlled by turning the chain length of PEG. Namely, the size of the HgS nanoparticles is decreased as the PEG with longer length is used.

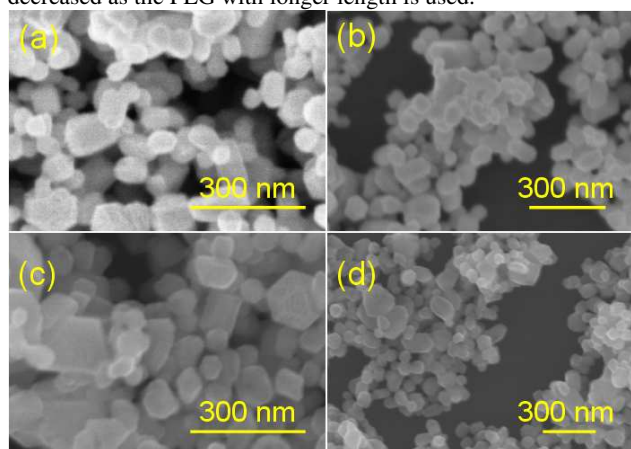


Fig. 4. SEM images of the as-prepared final HgS products with different PEG lengths (a) PEG-0, (b) PEG-2000, (c) PEG-4000, and (d) PEG-6000.

3.3 Growth mechanism of HgS nanoparticles.

In the synthesis, when $\text{Hg}(\text{NO}_3)_2$ and $\text{C}_2\text{H}_5\text{NS}$ are dissolved into the deionized water, a clear solution were obtained. As illustrated in Fig. 5, CH_3SNH_2 can be first hydrolysis to H_2S , which are easy to be further ionized into S^{2-} ions. Then, S^{2-} ions can directly react with Hg^{2+} ions and HgS clusters can be quickly formed, which will be used as the growth units. When the solution supersaturation, the crystal began to grow and the HgS monomers will be formed. It is known that the morphology of the as-prepared products can be determined by their crystal structures to some extents.¹⁹ The isotropic unit cell structure generally results in isotropic growth of particles and accordingly leads to spherical-like morphology of the products.²⁰ Therefore, after the initial nucleation, the HgS monomers can grow into relatively small nanocrystals. Driven by the minimization of surface energy, the HgS crystals have a tendency to grow bigger, resulting in a thermodynamics stable state. During this process, the surface of the as-growth HgS monomers could be easily absorbed by the nonionic PEG molecular, which will stabilize and protect the nanoparticle, and finally, the sphere-like morphology of HgS nanocrystals will be formed. The possible growth mechanism of HgS nanoparticles is schematically illustrated in Fig. 5. This is similar to the formation process of PbS and MoS_2 nanoparticles reported previously.^{21,22}

An interesting discovery is that the sizes of HgS nanoparticles are decreased as increasing the chain length of PEG (Fig. 4). The phenomenon can be understood as the following reasons:

(i) The shorter length of PEG can form stronger bonds than that of longer length.²³ According to Boltzmann distribution, the

stronger adsorption will provide a higher density of PEG on HgS crystal surrounding. The adsorbed PEG molecules will slow down the rate of growth units moving to the as-growing HgS crystal surface. This contribute to the growth units have enough time to move the lowest energy position. Thermodynamics plays a dominant role in this process, the whole system has the lowest energy, thus form the bigger particles. In comparison, the longer length PEG owns a weaker adsorption, the adsorption density of PEG on HgS surfaces is smaller, nucleating rate is increased, thus the relative smaller particle was formed.

(ii) The polarity of the PEG increases with decreasing the length of the carbon chain length, which causes the decrease of the nucleation rate of HgS resulting in the formation of bigger particles. Therefore, the reactivity of the ions in solution can be controlled by adjusting the PEG length in the mixed solvent. Longer PEG length leads to easier nucleation, greater reactivity of the reactants, and faster reaction rate, and thus a lack of time to age and produce crystals with small size and even assemble to irregular particles (Fig. 4D). Moreover, the fluid viscosity of the PEG with longer chains is higher than the shorter one, even though the nucleation does not change, the post growth will be suppressed obviously.

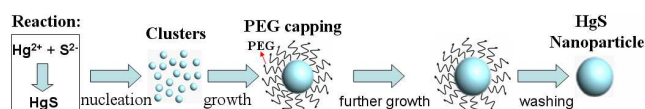


Fig. 5. Possible growth mechanism of the HgS nanoparticle.

3.4 Optical properties.

It is known that controlling the size of nanomaterial synthesis affords an opportunity to obtain samples with desirable optical performances.²⁴ In order to investigate the optical property of the obtained HgS nanoparticles, the UV-vis adsorption spectrum of the product is measured. Fig. 6 illustrates the DRS spectra of samples HgS-0, HgS-2000, HgS-4000, HgS-6000. The absorption edges of the HgS nanoparticles were found between 604 and 620 nm, corresponding to the absorption edge of a semiconductor material. The absorption edge for the samples from HgS-6000 to HgS-0 showed a small blue shift, which seems to be inconsistent with the general principle of the quantization size effect, namely the band-gap of semiconductors increases with decreasing in particle size.²⁵ The ratio of Hg/S was 1.07 and 1.03 by XPS and EDX measurements, as shown in Figures 2 and 3, which indicates that the obtained HgS samples are off stoichiometric and the high surface defects exist. These defects may be the real reason why the band gap is increasing with increasing size of the HgS nanoparticles.

By extrapolating the absorption edge using a linear fitting method, the band gap values of HgS nanoparticles were calculated (Table 1). The band gap values increased slightly from 2.00 to 2.05 eV as the particle size increased. The steep shape of the visible region reveals that the absorption band of HgS is due to the transition from the valence band to the conduction band²⁶ and is not due to the transition from the metal impurity level to the conduction band, as observed for metal-ion-doped semiconductors.²⁷ Thus, the steep absorption edge implies single-phase HgS, which is consistent with our XRD results. It is expected that the novel property of the HgS nanoparticles may

offer exciting opportunities for the potential application in infra-red emitters and catalysts.

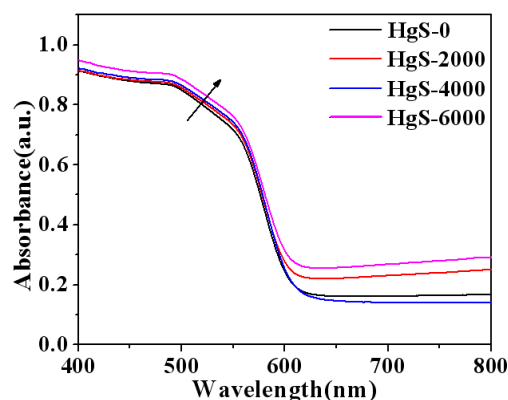


Fig. 6. UV-vis DRS spectrum of HgS nanoparticles with different PEG lengths.

Table 1. Band gap values of HgS nanoparticles calculated from DRS data.

Sample	Linear fit wavelength (nm)	Band gap (eV)
HgS-0	604.878	2.05
HgS-2000	607.843	2.04
HgS-4000	610.837	2.03
HgS-6000	620.000	2.00

3.5 Photocatalytic performance of HgS nanoparticles.

Methylene blue is one kind of organic dye and often used as a model pollutant to study the photocatalytic activity or performance of nanomaterials.²⁸ The maximum absorptive energy of methylene blue is at 664 nm. In this study, methylene blue was chosen as an object to investigate the photocatalytic degradation properties of the as-prepared HgS nanoparticles with the help of UV-vis absorption spectra. In Fig. 7, it is found that the absorptive intensity of methylene blue at 664 nm gradually decreases with a prolonging the irradiation time when the mixed solution of methylene blue and HgS nanoparticles was exposed to visible light irradiation by a sodium vapour lamp at high pressure and room temperature. This result indicates that methylene blue underwent degradation behavior under the catalysis of HgS nanocrystals. If the degradation ratio is defined as the ratio between the decreased absorptive intensity and that of the initial methylene blue solution, the degradation ratio is about 85% when the mixed solution was irradiated for 3 h. These imply that the as-synthesized HgS nanoparticles have good photocatalytic activity for methylene blue and are likely to be efficient photocatalysts in the applied field. As per the photocatalytic mechanism of HgS nanoparticles on methylene blue, we assume that the electron injection from photoexcited methylene blue molecules to HgS nanoparticles leads to a reduction of molecular oxygen and oxidative decomposition of the electron-deficient methylene blue. To the best of our knowledge, the photocatalytic performances of HgS nanoparticles have not been reported and the catalytic mechanism of HgS has not been well understood until now. In our future work, we will investigate the catalytic mechanism of HgS nanoparticles in detail.

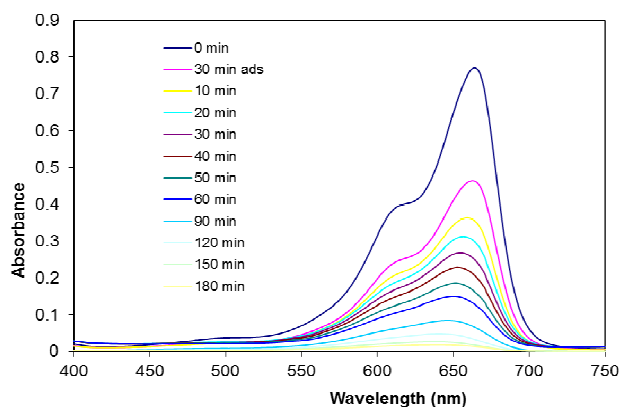


Fig.7 Time-dependent UV-Vis absorption spectra of methylene blue (5mg/L) degradation in HgS nanoparticles under visible light irradiation.

4. Conclusion

In summary, we have reported a simple hydrothermal method to prepare HgS nanoparticles using PEG as stabilizing agent and characterized by a variety of methods. The XRD analysis confirmed that the HgS nanoparticles are in hexagonal phase. SEM and TEM analysis revealed the nanoparticles with an average size from 55 to 35 nm. On the basis of the structural and morphological studies, a growth mechanism has been proposed to explain the formation of the HgS nanoparticle. The UV-vis DRS measurements confirmed that the samples have the band gap from 2.00 to 2.05 eV and slightly change upon changing the size of HgS nanoparticles. The HgS nanoparticles exhibited good photocatalytic activity for the degradation of MB aqueous solution under visible-light illumination. Because of their hydrothermal synthesis and controlled morphology, the obtained HgS nanoparticles have the potential applications in catalysis.

This work was supported by Sultan Qaboos University Internal Grant (Grant No.: IG/SCI/Dean/14/01).

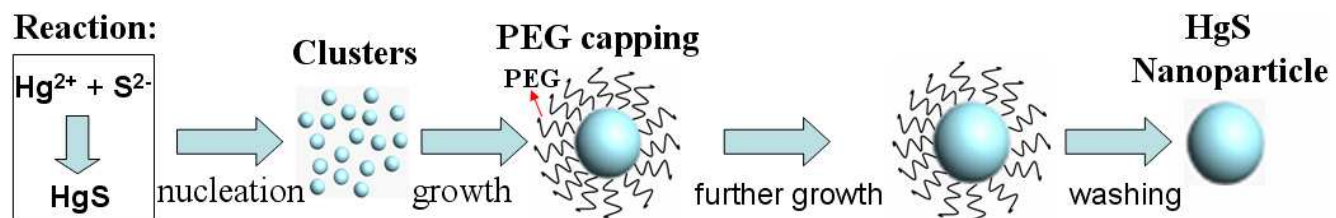
References

- ^a Department of Chemistry, College of Science, Sultan Qaboos University, Muscat, Sultanate of Oman.
- ^b College of Chemistry and Life Science, Shenyang Normal University, Shenyang, 110034, China.
- ^c Laboratory of Green Chemistry, LUT Savo Sustainable Technologies, Lappeenranta University of Technology, Sammonkatu 12, FI-50130 Mikkeli, Finland.
- ^d Department of Chemical Engineering, Kwangwoon University, Seoul 139-701, Korea.
- ^e Department of Materials and Environmental Chemistry, Arrhenius Laboratory, Stockholm University, S-106 91 Stockholm, Sweden.
- *Corresponding author Tel: +968-2414 2436;
e-mail: srengaraj1971@yahoo.com
- [1] (a) L. Shi, A. J. T. Naik, J. B. M. Goodall, C. Tighe, R. Gruar, R. Binions, I. Parkin and J. Darr, *Langmuir*, 2013, **29**, 10603; (b) N. S. Porter, H. Wu, Z. W. Quan and J. Y. Fang, *Acc. Chem. Res.*, 2013, **46**,

- 1867; (c) W. Wichiansee, M. N. Nordin, M. Green and R. J. Curry, *J. Mater. Chem.*, 2011, **21**, 7331; (d) E. Wetterskog, C. W. Tai, J. Grins, L. Bergström and G. Salazar-Alvarez, *ACS Nano*, 2013, **7**, 7132.
- [2] (a) S. Rengaraj, S. Venkataraj, C. Tai, Y. H. Kim, E. Repo and M. Sillanp, *Langmuir*, 2011, **27**, 5534; (b) X. Liu, R. Liu, Y. R. Tang, L. C. Zhang, X. D. Hou and Y. Lv, *Analyst*, 2012, **137**, 1473.
- [3] X. Zhang and M. Takeuchi, *Angew. Chem., Int. Ed.*, 2009, **48**, 1.
- [4] I. Bilecka and M. Niederberger, *Nanoscale*, 2010, **2**, 1358.
- [5] (a) A. Drott, E. Björn, S. Bouchet and U. Skyllberg, *Environ. Sci. Technol.*, 2013, **47**, 4197; (b) F. Pietra, R. J. A. van Dijk-Moes, X. X. Ke, S. Bals, G. V. Tendeloo, C. D. M. Donega and D. Vanmaekelbergh, *Chem. Mater.*, 2013, **25**, 3427.
- [6] N. Goswami, A. Giri, S. Kar, M. S. Bootharaju, R. John, P. L. Xavier, T. Pradeep and S. K. Pal, *Small*, 2012, **8**, 3175.
- [7] N. Tokyo, *J. Appl. Phys.*, 1975, **46**, 4857.
- [8] R. S. Davidson and C. J. Willsher, *Nature*, 1979, **21**, 238.
- [9] (a) H. D. Riccius and K. J. Siemsen, *J. Chem. Phys.*, 1970, **52**, 4090; (b) A. Ben-Moshe, A. O. Govorov and G. Markovich, *Angew. Chem. Int. Ed.* (2013), **52**, 1275.
- [10] (a) N. Tokyo, K. Azkio, *Jpn. Kokai Patent*, 7855478, 1978; (b) M. Perakh, H. Ginsberg, *Thin Solid Films*, 1978, **52**, 195; (c) R.S. Patil, T. P. Gujar, C. D. Lokhande, R. S. Mane, Sung-Hwan Han, *Solar Energy*, 2007, **81**, 648.
- [11] K. A. Higginson, M. Kuno, J. Bonevich, S. B. Qadri, M. Yousuf and H. Mattoussi, *J. Phys. Chem. B*, 2002, **106**, 9982.
- [12] (a) Y. D. Li, Y. Ding, H. W. Liao and Y. T. Qian, *J. Phys. Chem. Solids*, 1999, **60**, 965; (b) H. Wang, J. R. Zhang and J. J. Zhu, *J. Cryst. Growth*, 2001, **233**, 829.
- [13] J. H. Zeng, J. Yang and Y. T. Qian, *Mater. Res. Bull.*, 2001, **36**, 343.
- [14] X. J. Zhang, Y. Xie, Q. R. Zhao and Y. P. Tian, *New J. Chem.*, 2003, **27**, 827.
- [15] X. Y. Chen, X. Wang, Z. H. Wang, X. G. Yang and Y. T. Qian, *Cryst. Growth & Des.*, 2005, **5**, 347.
- [16] M. W. Shao, L. F. Kong, Q. Li, W. C. Yu and Y. T. Qian, *Inorg. Chem. Commun.*, 2003, **6**, 732.
- [17] H. Wang and J. J. Zhu, *Ultrasonics Sonochemistry*, 2004, **11**, 293.
- [18] T. Ren, S. Xu, W. B. Zhao and J. J. Zhu, *Journal of Photochemistry and Photobiology A: Chemistry*, 2005, **173**, 93.
- [19] W. M. Du, X. F. Qian, X. S. Niu and Q. Gong, *Cryst. Growth Des.*, 2007, **7**, 2733.
- [20] X. C. Duan, X. D. Liu, Q. Chen, H. B. Li, J. Li, X. Hu, Y. Y. Li, J. M. Ma, W. J. Zheng, *Dalton Trans.*, 2011, **40**, 1924.
- [21] S. F. Wang, F. Gu and M. K. Lu, *Langmuir*, 2006, **22**, 398.
- [22] Z. Z. Wu, D. Z. Wang and A. Sun, *J. Mater. Sci.*, 2010, **45**, 182.
- [23] K. Letchford and H. Burt, *European Journal of Pharmaceutics and Biopharmaceutics*, 2007, **65**, 259.
- [24] X. G. Peng, L. Manna, W. D. Yang, J. Wichham, E. Scher, A. Kadavanich and A. P. Alivisatos, *Nature*, 2000, **404**, 59.
- [25] S. Tawkaew, Y. Fujishiro, S. Yin and T. Sato, *Colloids Surf. A*, 2001, **179**, 139.
- [26] I. Tsuji, H. Kato, A. Kudo, *Chem. Mater.*, 2006, **18**, 1969.
- [27] (a) I. Tsuji and A. Kudo, *J. Photochem. Photobiol. A*, 2003, **156**, 249; (b) D. W. Hwang, H. G. Kim, J. S. Lee, J. Kim, W. Li and S. H. Oh, *J. Phys. Chem. B*, 2005, **109**, 2093.
- [28] W. Ho, J. C. Yu, J. Lin, J. Yu. and P. Li, *Langmuir*, 2004, **20**, 5865.

Graphical Abstract

For Table of Contents Use Only



HgS nanoparticles have been synthesized by a hydrothermal method using polyethylene glycol (PEG) as stabilizing agent. The as-prepared HgS nanomaterials show good photocatalytic behaviour.

Supporting information

A simple hydrothermal route for the preparation of HgS nanoparticles and their photocatalytic activities

Rengaraj Selvaraj^{a*}, Kezhen Qi^b, Salma M. Z. Al-Kindy^a, Mika Sillanpää^c, Younghun Kim^d,
Cheuk-wai Tai^e

^a *Department of Chemistry, College of Science, Sultan Qaboos University, Muscat, Sultanate of Oman.*

^b *College of Chemistry and Life Science, Shenyang Normal University, Shenyang, 110034, China.*

^c *Laboratory of Green Chemistry, LUT Savo Sustainable Technologies, Lappeenranta University of Technology, Sammonkatu 12, FI-50130 Mikkeli, Finland.*

^d *Department of Chemical Engineering, Kwangwoon University, Seoul 139-701, Korea.*

^e *Department of Materials and Environmental Chemistry, Arrhenius Laboratory, Stockholm University, S-106 91 Stockholm, Sweden.*

Corresponding Author: Dr. Rengaraj Selvaraj

Address: *Department of Chemistry, College of Science, Sultan Qaboos University, Muscat, Sultanate of Oman.*

*Corresponding author Tel: +968-2414 2436;

e-mail: srengaraj1971@yahoo.com

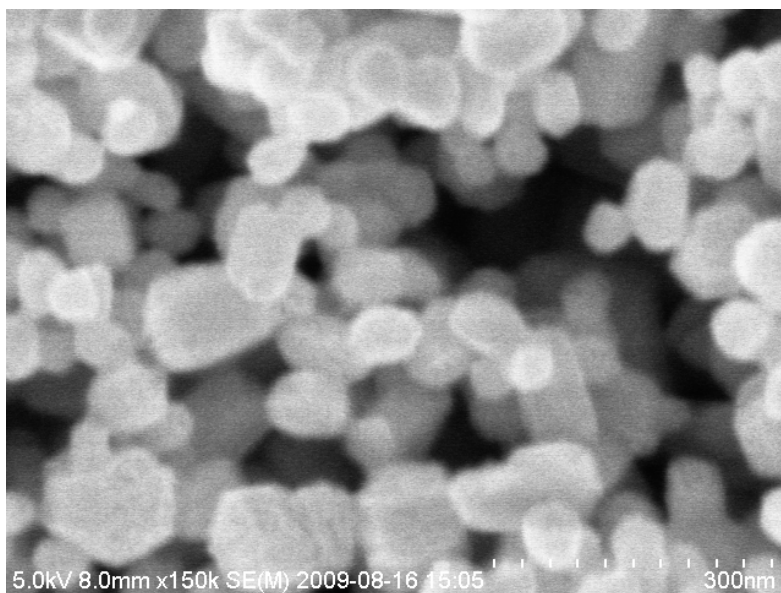


Fig. S1. SEM image of the as-prepared HgS products with the assistance of PEG-0.

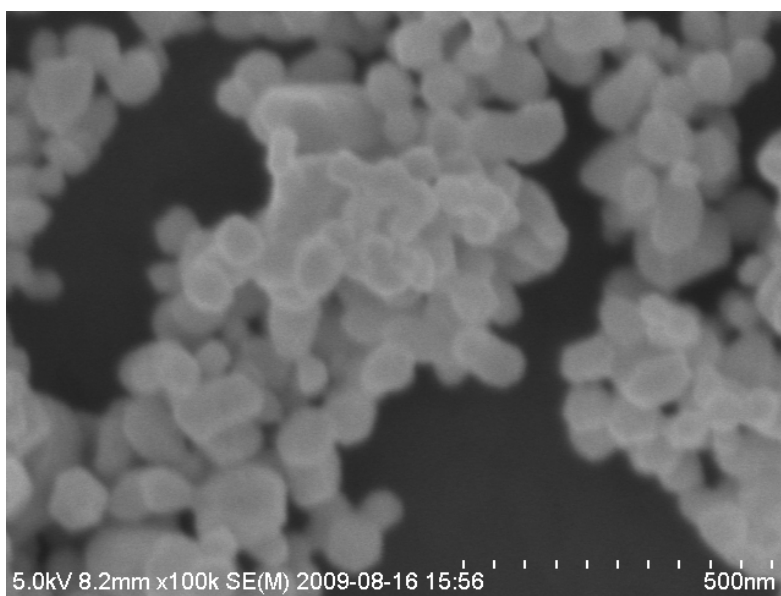


Fig. S2. SEM image of the as-prepared HgS products with the assistance of PEG-2000.

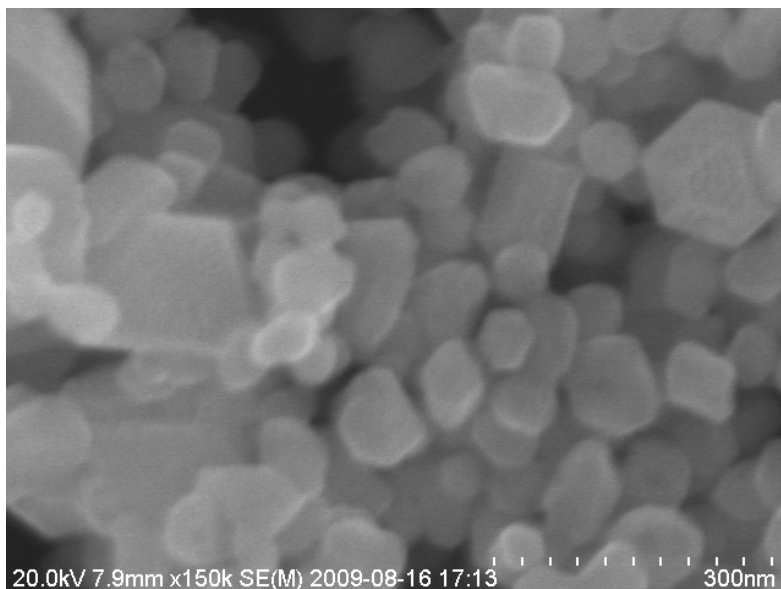


Fig. S3. SEM image of the as-prepared HgS products with the assistance of PEG-4000.

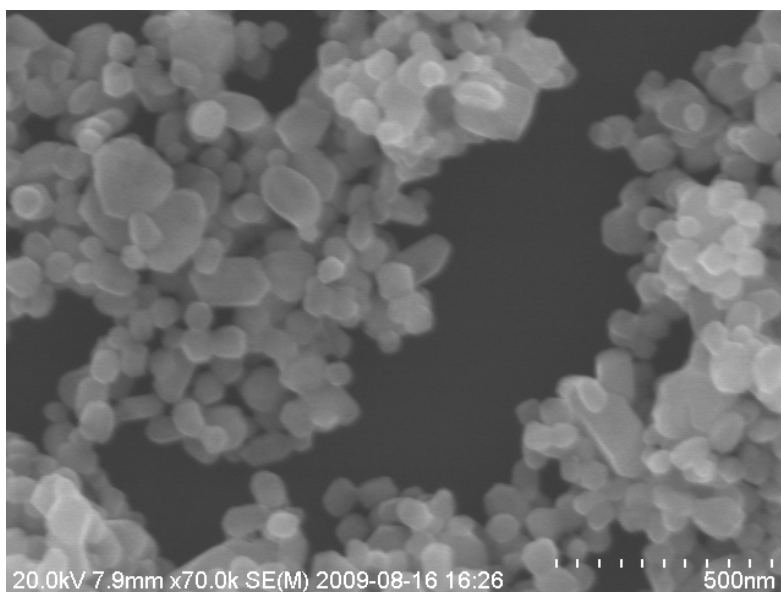


Fig. S4. SEM image of the as-prepared HgS products with the assistance of PEG-6000.